The Astrophysical Journal, 743:178 (9pp), 2011 December 20 doi:10.1088/0004-637X/743/2/178

HIGH-CONTRAST STELLAR OBSERVATIONS WITHIN THE DIFFRACTION LIMIT AT THE PALOMAR HALE TELESCOPE

B. Mennesson[1], C. Hanot[2], E. Serabyn[1], K. Liewer[1], S. R. Martin[1], and D. Mawet[3]
[1] Jet Propulsion Laboratory, California Institute of Technology, 4800 Oak Grove Drive, Pasadena, CA 91109-8099, USA; bertrand.mennesson@jpl.nasa.gov
[2] AEOS, University of Liège, Allée du 6 Août, 17 Bât B5c, B-4000 Liège, Belgium
[3] European Southern Observatory, Alonso de Cordova 3107, Vitacura, Santiago, Chile
Received 2011 August 19; accepted 2011 October 26; published 2011 December 2

ABSTRACT

We report on high-accuracy high-resolution (<20 mas) stellar observations obtained with the Palomar Fiber Nuller (PFN), a near-infrared ($\simeq$2.2 μm) interferometric coronagraph installed at the Palomar Hale telescope. The PFN uses destructive interference between two elliptical (3 m × 1.5 m) sub-apertures of the primary to reach high dynamic range inside the diffraction limit of the full telescope. In order to validate the PFN's instrumental approach and its data reduction strategy, based on the newly developed "Null Self-Calibration" (NSC) method, we observed a sample of eight well-characterized bright giants and supergiants. The quantity measured is the source astrophysical null depth, or equivalently the object's visibility at the PFN 3.2 m interferometric baseline. For the bare stars α Boo, α Her, β And, and α Aur, PFN measurements are in excellent agreement with previous stellar photosphere measurements from long baseline interferometry. For the mass-losing stars β Peg, α Ori, ρ Per, and χ Cyg, circumstellar emission and/or asymmetries are detected. Overall, these early observations demonstrate the PFN's ability to measure astrophysical null depths below 10^{-2} (limited by stellar diameters), with 1 σ uncertainties as low as a few 10^{-4}. Such visibility accuracy is unmatched at this spatial resolution in the near-infrared and translates into a contrast better than 10^{-3} within the diffraction limit. With further improvements anticipated in 2011/2012, a state-of-the-art infrared science camera and a new extreme adaptive optics system, the PFN should provide a unique tool for the detection of hot debris disks and young self-luminous sub-stellar companions in the immediate vicinity of nearby stars.

Key words: circumstellar matter – infrared: stars – instrumentation: high angular resolution – stars: individual (α Boo, α Her, β Peg, β And, α Ori, ρ Per, α Aur, χ Cyg)

Online-only material: color figures

1. INTRODUCTION

High contrast at high angular resolution is required in various fields of astrophysics, notably for the direct imaging and spectroscopic characterization of exoplanetary systems, where faint planets or debris disks are located in the close vicinity ($\simeq$0.1–$\simeq$5 AU) of their much brighter parent stars. While a few recent detections have been made in the favorable case of young self-luminous exoplanets in relatively wide orbits (e.g., Kalas et al. 2008; Marois et al. 2008), the inner planet-forming region remains unexplored at high contrast.

Near-infrared coronagraphs working with current-generation adaptive optics (AO) systems mounted on large (diameter $D \geqslant 5$ m) ground-based telescopes have inner working angles limited to 300 mas or more. In the case of traditional Lyot coronagraphs (Liu et al. 2009; Hinkley et al. 2007), this limit is directly fixed by the size of the occulting focal plane mask. In the case of phase coronagraphs, the current practical resolution limit for high-contrast (say 10^{-4} or better) imaging at near-infrared wavelengths on large telescopes is also $\simeq$5–10 λ/D because of residual wavefront errors (Boccaletti et al. 2004). Operation closer to the axis ($\simeq \lambda/D$) is only possible with extreme AO, as demonstrated by observations with a 1.5 m diameter well-corrected sub-aperture (Serabyn et al. 2010). Future coronagraphs such as Spectro-Polarimetric High-contrast Exoplanet Research Instrument (SPHERE; Boccaletti et al. 2008) and Gemini Planet Imager (GPI; Marois et al. 2008), using extreme AO on large 8 m telescopes, will soon allow improved performance close to the optical axis. However, even with these next-generation instruments, high contrast in the near-infrared will only be available at $\simeq$2–3 λ/D.

Near-infrared interferometry operates in a very different angular regime. The resolution ranges from 20 to 30 mas when using sub-apertures of 5–8 m telescopes, to $\leqslant$1 mas using separate telescopes. However, due to calibration difficulties, the contrast of ground-based interferometers, whether relying on visibility or phase closure measurements, has so far been limited to a few 10^{-3} at best (Absil et al. 2006; Colavita et al. 2009; Duvert et al. 2010; Zhao et al. 2008). Clearly, some new advances are needed in order to bridge the traditional gap between coronagraphs, limited in angular resolution, and long baseline interferometers, limited in dynamic range.

This is the object of the fiber nulling technique, which allows deep cancellation of the on-axis light gathered by two (or more) apertures, and the detection of faint nearby sources. In principle, the approach can be applied equally to long baseline interferometers or to sub-apertures of a large telescope. The first verification of deep nulling using this technique was reported by our group using monochromatic visible light (Haguenauer & Serabyn 2006), and then broadband near-infrared light in H (Mennesson et al. 2006) and K (Martin et al. 2008) bands. In the simple case of two beams, the principle is to combine them into a single-mode fiber while maintaining a differential π phase shift. Co-axial and multi-axial (as in the Palomar Fiber Nuller (PFN)) recombination schemes both work, as long as the various beams are finally injected into a common single-mode fiber. Since the individual-aperture wavefronts are spatially filtered by the fiber, the accessible cancellation level is primarily fixed by the residual optical path difference (OPD) between the two apertures, and

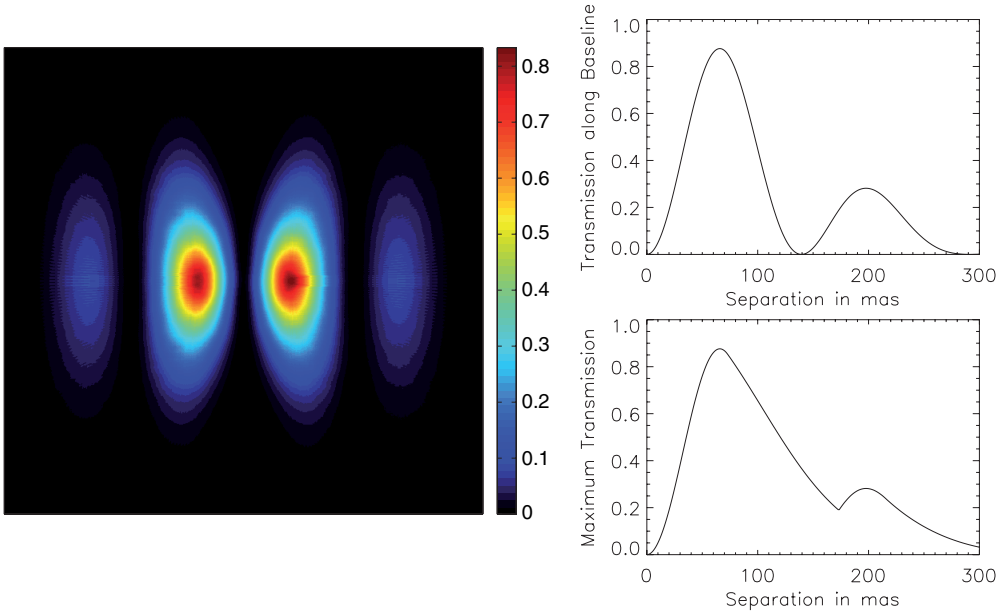

Figure 1. Left: PFN sky transmission (north is up, east is to the left) over a 0.″6 × 0.″6 field of view, assuming a purely east–west 3.20 m baseline separating two elliptical sub-apertures (3 m × 1.5 m). Top right: PFN transmission vs. separation, cut along baseline direction. Bottom right: maximum PFN transmission vs. separation (baseline orientation angle chosen to maximize transmission at any given separation).

(A color version of this figure is available in the online journal.)

not by the individual wavefront errors (Mennesson et al. 2002a). This fundamental property allows the occurrence of frequent deep quasi-instantaneous (a few ms) cancellation levels, even for stellar wavefronts characterized by the Strehl ratio of current AO systems (≃50% at *K* band). Nulling two apertures of diameter d separated by a distance b, on-axis sources are cancelled out, while the half power transmission point corresponds to an off-axis separation $\lambda/4b$, providing sensitivity to sources well within the diffraction limit of single telescopes. The field of view is limited by the single-mode fiber to $\simeq\lambda/d$ at FWHM.

As an initial validation of the technique on the sky, we have installed a fiber nulling system on a single telescope, at the Palomar 200 inch telescope. The PFN was built as a basic physics demonstrator, and so is initially restricted to the observations of very bright stars by its modest detector. After a presentation of the optical set-up, we detail the observing methodology and the data reduction strategy specifically developed for the PFN. Finally, as a validation of the technique against existing measurements, we present results obtained in 2008 and 2009 on eight well-known giant and supergiant stars.

2. OPTICAL SET-UP AND METHODOLOGY

A full description of the PFN hardware is given in a recent technical design and performance paper (Martin et al. 2008). The PFN system observes in K_s band (≃2.2 μm) and uses two elliptical 3 m × 1.5 m sub-apertures located a distance $b = 3.20$ m apart. Its sky transmission pattern is represented in Figure 1, showing a 50% transmission point at 35 mas, to be compared with the 200 mas FWHM sub-aperture field of view and the full telescope 90 mas point-spread function. In essence, a fiber nuller system mounted on a large telescope offers a natural complement to a traditional coronagraph: from a resolution standpoint, it starts working where a regular coronagraph stops and vice versa. In fact, when used on a single telescope, a fiber nuller system could in principle be fed by an optical stop reflecting the very central part of the field (e.g., inner 2–3 λ/D) and hence work in conjunction with a regular coronagraph.

The PFN optical set-up is illustrated in Figure 2 (adapted from Martin et al. 2008). It is mounted on a standalone 4′ × 2′ bread-board inserted downstream of the Palomar AO system. Under average seeing conditions and for the bright stars considered here, the AO system (Troy et al. 2000) delivers to the PFN an input wavefront with a typical 200–250 nm rms error in the *K* band. The AO system can be thought of as a first-order fringe tracker, maintaining the relative phase difference between the two beams to be nulled. After the AO bench, a fold mirror delivers the $f/16$ converging beam to the PFN. After collimation, the stellar beam first goes through a "K-mirror" used to rotate the pupil with respect to the PFN. The beam subsequently goes through a fixed mask with two elliptical holes defining the fiber nuller sub-apertures and interferometric baseline. A "split" mirror allows independent control of the two beams, (denoted "A" and "B") optical path lengths and directions. A common dichroic plate inserted into the two sub-beams allows angle tracking at *J* band (in 2008) or using visible/red light (in 2009). The K_s-band science beams go through a spatial chopper providing sequential measurements of dark ("D," including detector and background contributions), interferometric ("A+B") and individual ("A", "B") beam intensities (Figure 3) over cycles of ≃200 ms. A chevron-shaped piece of Infrasil glass reduces the spacing between the two science beams and allows better injection efficiency into the fiber (typically 40%). Since the split mirror can only introduce a π phase shift at a single wavelength, the chevron is also slightly rotated to introduce a constant differential glass thickness between the beams, optimized to generate a quasi-achromatic π phase shift over the finite PFN bandpass. This broadband cancellation technique (Angel et al. 1997) has already been demonstrated successfully for the Keck Interferometer Nuller (Mennesson et al. 2003). Finally, a common off-axis parabola is used for recombination, injecting the two beams into a single-mode fiber. The fiber output is then re-imaged onto a fast single-pixel infrared (InGaAs) photometer.

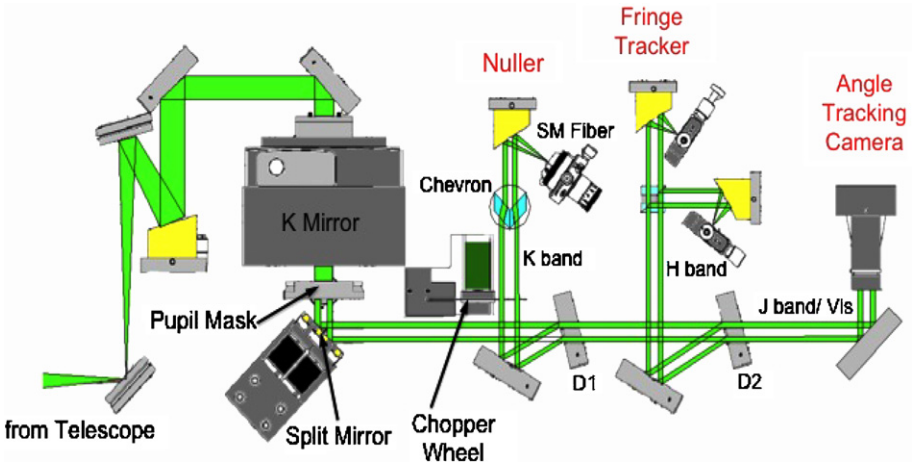

Figure 2. Palomar Fiber Nuller optical layout. The pupil rotator ("K mirror") rotates the image of the fixed pupil mask on the telescope primary. The *K*-band part of the light is reflected off a first dichroic ("D1"), goes through a 4-position chopper wheel, and is then injected into a single-mode fiber. The fiber output is then detected on a single pixel photometer (not shown). A second dichroic ("D2") reflects the *H*-band light, which is planned to be used for fringe tracking, and transmits shorter wavelengths which are used for angle tracking. The angle tracking camera (*J* band in 2008, visible/red in 2009) stabilizes individual beam pointing and injection into the *K*-band single-mode fiber. See the text for more details.

(A color version of this figure is available in the online journal.)

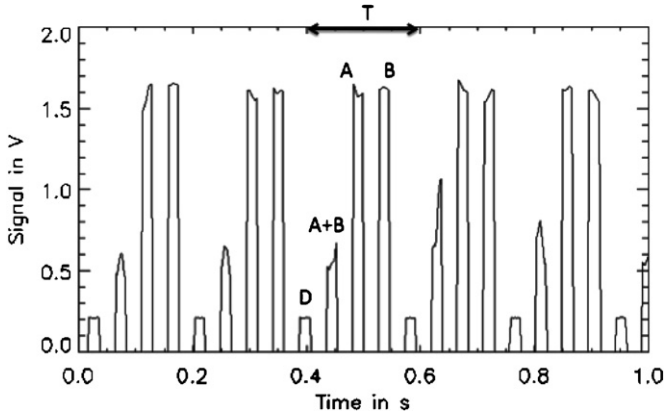

Figure 3. Chopped signal recorded on α Her. Cycle period: $T = 186$ ms, sampling interval = 2 ms. Five successive cycles are shown, each with alternate measurements of dark ("D," including detector and background contributions), interferometric ("A+B"), and individual ("A," "B") beam intensities. Data recorded during transitions have been discarded.

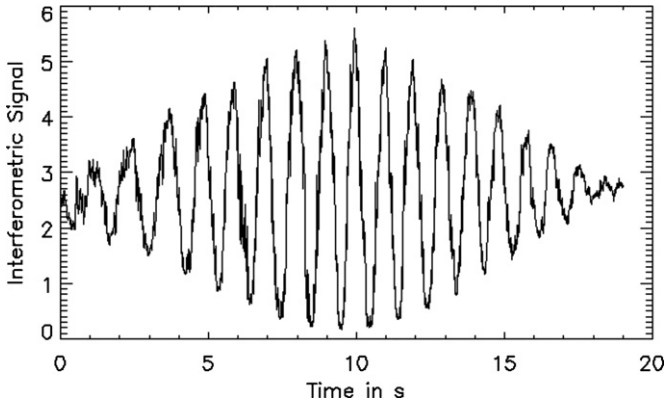

Figure 4. Fringe scan recorded on α Her by varying the OPD in one arm of the PFN (raw data sampled every 10 ms). AO correction and further angle tracking typically stabilize the individual beam photometry at the 3%–10% rms level over five minutes. Such interferograms are used to locate the central fringe (best null) position.

For a given target, the observations start by optimizing the flux injected into the fiber for each of the two sub-beams using the two tip–tilt mirrors in the split mirror. While the stellar position is maintained on the angle tracking camera (*J* band), the OPD between the beams is scanned via a piezoelectric transducer-driven mirror (split mirror), and a broadband interferogram is recorded on the *K*-band detector (Figure 4). This fringe scan allows the determination of the central dark fringe (deepest broadband null) position and the split mirror OPD is set at this "null" position. Typically 1–5 minute long chopped sequences—as described above—are then recorded per target. In the cases of α Her and β Peg, the K-mirror was rotated to provide different baseline orientations on the sky to begin to test the baseline rotation and signal modulation aspects.

3. PFN OBSERVABLES AND DATA REDUCTION

Given a series of $\simeq 200$ ms long chop cycles (Figure 3), each consisting of successive dark ("D"), interferometric ("A+B") and individual ("A," "B") measurements, one computes the quantities

$$\hat{I}_N(t) = (A+B)(t) - \hat{D}(t) \quad (1)$$

$$\hat{I}_1(t) = A(t) - \hat{D}(t) \quad (2)$$

$$\hat{I}_2(t) = B(t) - \hat{D}(t) \quad (3)$$

$$\hat{I}_P(t) = \hat{I}_1(t) + \hat{I}_2(t) + 2\sqrt{\hat{I}_1(t).\hat{I}_2(t)} \quad (4)$$

$$\hat{N}_{\rm Obs}(t) = \frac{\hat{I}_N(t)}{\hat{I}_P(t)}. \quad (5)$$

Within a given cycle, $(A+B)(t)$ is the instantaneous interferometric signal (close to null) recorded every 2 ms, while $\hat{D}(t)$ is the average dark level measured during the same cycle. $\hat{I}_N(t)$, $\hat{I}_1(t)$, $\hat{I}_2(t)$ and $\hat{I}_P(t)$ serve as estimates of the instantaneous null, peak and individual stellar signals $I_N(t)$, $I_P(t)$, $I_1(t)$ and $I_2(t)$ at the time of an (A+B) interferometric measurement. $\hat{N}_{\rm Obs}(t)$ is the estimated normalized instantaneous null depth, the final observable derived from the measured chopped signals.

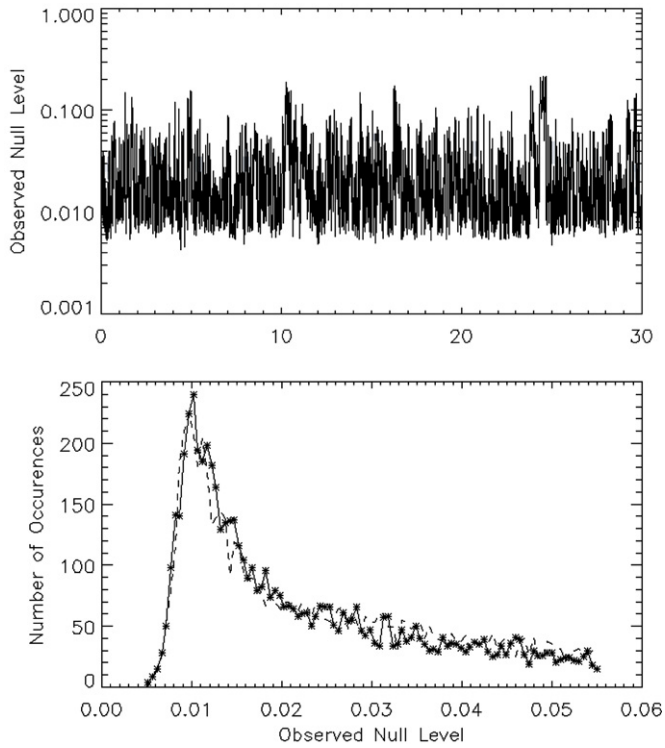

Figure 5. Top: null sequence obtained on β Peg (typical results, 2009 July) vs. time in seconds. Bottom, plain curve: observed null depth histogram. Bottom, dashed curve: best-fit model null histogram. The best-fit parameters are $N^a = 0.0089 \pm 0.0004$, mean differential phase = 0.29 rad, differential phase rms = 0.48 rad. Best fit $\chi^2 = 1.12$.

In the case of the PFN, the two beams are injected into a *common* single-mode fiber. Neglecting any differential polarization effects in the beam train, the recorded interferometric signal can be approximated by

$$(A+B)(t) = I_1(t) + I_2(t) + 2|V| \,.\, \sqrt{I_1(t) I_2(t)} \,.\, \cos(\phi(t) + \phi_V) + D(t), \quad (6)$$

where $|V|$ is the complex modulus of the source visibility at the PFN's baseline, ϕ_V its phase (zero for a symmetric and/or mostly unresolved source), and $\phi(t)$ the instantaneous differential phase between the beams. Writing $\phi(t) + \phi_V = \pi + \Delta\phi(t)$, where $\Delta\phi(t)$ is the phase offset from null, and using Equations (1)–(6), $\hat{N}_{\rm Obs}(t)$ can be theoretically modeled as

$$N_{\rm Theo}(t) = \frac{I_1(t) + I_2(t) - 2|V| \,.\, \sqrt{I_1(t) I_2(t)} \,.\, \cos(\Delta\phi(t))}{\hat{I}_P(t)} + \frac{(D(t) - \hat{D}(t))}{\hat{I}_P(t)}. \quad (7)$$

As detailed previously (Hanot et al. 2011), the PFN data reduction consists in fitting the *distribution* of observed null values $\hat{N}_{\rm Obs}(t)$ by the *distribution* of theoretical null values $N_{\rm Theo}(t)$. Because the quantity of interest is now the null distribution rather than its instantaneous value, we can replace the unknown instantaneous stellar intensity signals $I_{1,2}(t)$ of Equation (7) by their values estimated at a slightly later time: $\hat{I}_{1,2}(t)$. This is the principle of the numerical "Null Self-Calibration" (NSC) method, which is fully described by Hanot et al. (2011) and is used for all results reported here.

An essential characteristic of this analysis is that when modeling the *entire* distribution of observed null values, one can very effectively separate instrumental effects—such as fast intensity and OPD fluctuations—from the underlying object's visibility V, or equivalently its astrophysical null depth N^a defined as

$$N^a = \frac{1 - |V|}{1 + |V|}, \quad (8)$$

The astrophysical null depth is derived by minimizing a goodness-of-fit χ^2 test comparing the observed null distribution to the theoretical model distribution. The error bar (1σ confidence interval) on N_a is derived as explained in Hanot et al. (2011, Section 2.4). It is the largest of the uncertainties derived using two different methods: a regular χ^2 statistical analysis (strictly valid for a zero mean Gaussian noise) and a bootstrapping analysis. As a typical example, Figure 5 shows a null sequence and the result of a null distribution fit for PFN observations of β Peg. The agreement between the observed and best-fit modeled distributions is generally excellent, with reduced χ^2 consistently around unity for all observations reported hereafter, making us confident that the modeling approach is sound.

We described the NSC method and presented a first analysis of its applicability to the PFN data in Hanot et al. (2011). This previous work concentrated on observations of α Boo, showing that the derived null depths were extremely reproducible, and suggesting that any bias, if present at all in these particular measurements, is at the few 10^{-4} level or lower. A major advantage of the NSC method is then that, to first order, no observations of calibrator stars are needed to estimate the instrumental effects. In the following section, we seek to confirm this result on a larger sample of stars observed with the PFN, and better establish the current accuracy of the method.

4. RESULTS AND INTERPRETATION

We carried out astronomical test observations of resolved giants and supergiants already well characterized by long baseline interferometry (LBI) at 2.2 μm, some of them with previously detected excess emission above the photosphere. Our objective here is to explore the consistency of our measurements with values reported by LBI, i.e., quantify our measurement accuracy and assess potential biases.

Table 1 summarizes the astrophysical nulls measured by the PFN on eight stars over five nights: 2008 July 21, 2008 November 11 and 12, and 2009 July 10 and 11. The 2009 data were obtained with an upgraded angle tracking camera and an achromatic beam recombination system, providing better null accuracy (typically 0.1% rms or better). To interpret the measurements, we use the relationships established in the Appendix, which link the observed astrophysical null depth to the source physical characteristics in a few simple cases: uniform disks, limb darkened (LD) disks and binary systems.

As discussed in Hanot et al. (2011), some instrumental parameters can also be derived from the observed null distributions, in particular the residual phase jitter after AO correction. The derived K_s-band phase jitter ranges from 0.3 rad ($\simeq$100 nm) rms under good seeing conditions (2009 July) to 0.6 rad ($\simeq$200 nm) rms under bad seeing conditions (2008 November). Taking into account the spatial averaging of the phase over each sub-aperture, these figures are well aligned with the AO performance, which predicts a typical residual

Table 1
Summary of PFN Observations of Giants and Supergiants

Star	Type	Az	N_m^a	σ_m	N_p^a	σ_p	Excess	Date	Chop
α Boo	K1.5III	117	0.0132	1.3×10^{-4}	0.0131	0.0001	No	07/10/09	y/n
α Her	M5Iab	117	0.0306	0.0010	0.0326	0.0014	No	07/10/09	y/n
		72	0.0335	0.0010	0.0326	0.0014	No	07/10/09	n
		162	0.0333	0.0010	0.0326	0.0014	No	07/10/09	n
		all	0.0325	0.0016	0.0326	0.0014	No	07/10/09	y/n
β And	M0III	57	0.0070	0.0009	0.0062	0.0002	No	07/11/09	y
α Aur	G8III + G1III	72	0.052	0.004	0.051	<0.001	No	11/12/08	n
β Peg	M2.5II-III	87	0.0089	0.0004	0.0084	0.0002	No	07/10/09	y
		117	0.0113	0.0007	0.0084	0.0002	Yes	07/11/09	y
		all	0.0095	0.0011	0.0084	0.0002	No	07/11/09	y
α Ori	M2Iab	117	0.081	0.004	0.060	0.0003	Yes	11/11/08	y/n
ρ Per	M4II	117	0.074	0.007	0.0084	0.0002	Yes	11/12/08	y
χ Cyg	S Mira	117	0.029	0.0025	0.017	<0.001	Yes	07/21/08	n

Notes. Az is the baseline azimuth measured in degrees east of north. Circumstellar excess is reported when the astrophysical null N_m^a measured by the PFN is at least 3 σ above the "photospheric" null N_p^a predicted for naked stars by LBI. $\sigma = \sqrt{\sigma_m^2 + \sigma_p^2}$, where σ_m and σ_p indicate the uncertainties on the measured PFN nulls and on the predicted photospheric nulls, respectively. Date format is dd/mm/yy. The "chop" column indicates whether fast chopping between the beams was enabled during the observations. 2009 data exhibit better accuracy thanks to hardware improvements. Targets labeled in italic (β *Peg,* α *Ori,* ρ *Per*, and χ *Cyg*) are variable mass-losing stars. All four show significant excess emission in the PFN measurements, while none of the other stars does.

wavefront rms error of 200–250 nm over the full telescope aperture.

4.1. Individual Results: Naked Stars

4.1.1. α Boo

α Boo is a bright K1.5 III giant, on which we gathered our most extensive data set: five independent null sequences recorded over an hour at the same baseline (no rotation). We have analyzed it in a previous paper (Hanot et al. 2011) and derived an astrophysical null depth of $1.32 \times 10^{-2} \pm 1.3 \times 10^{-4}$. The error bar quoted here comes purely from propagating the statistical errors determined on each individual measurement, assuming that each of them is affected by a zero mean Gaussian noise, i.e., that there are no systematic errors (Hanot et al. 2011). Using the linear limb darkening coefficient of 0.350 predicted in the K band for a 4300 K giant star with $\log g = 2.0$ (Claret et al. 1995) and Equation (A4), the LD diameter derived from the PFN null measurement is then 20.95 mas $\pm$ 0.11 mas. This value is in excellent agreement with the LD diameter of 20.91 mas $\pm$ 0.08 mas previously measured by LBI with FLUOR/IOTA[4] (Perrin et al. 1998), which corresponds to an astrophysical null depth of $1.31 \times 10^{-2} \pm 1 \times 10^{-4}$ at the PFN 3.20 m baseline.

4.1.2. α Her

α Her is a very bright M5 supergiant that we observed at three different baseline rotation angles (a single measurement was obtained at each angle). The measured astrophysical null depth shows slight variation versus azimuth angle, at the 1.5σ level, which is not statistically significant. Averaging over the observed azimuth angles, we find an average null depth of $3.25 \times 10^{-2} \pm 1.6 \times 10^{-3}$. The final error bar quoted here is significantly larger than on α Boo, reflecting the observed null fluctuations versus azimuth, the smaller number of observations, and some seeing degradation. Using the linear limb darkening coefficient of 0.436 predicted for α Her physical characteristics (Claret et al. 2000), the LD diameter derived from the PFN null measurement is 33.10 mas $\pm$ 0.81 mas. This value is in excellent agreement with the LD diameter of 33.14 mas $\pm$ 0.76 mas measured by LBI with FLUOR/IOTA (Perrin et al. 2004), which would imply a null of $3.26 \times 10^{-2} \pm 1.4 \times 10^{-3}$ at the PFN baseline.

We thus have no evidence for the companion previously detected by visible speckle interferometry (McAlister et al. 1993). However, we can derive upper limits on the K-band flux of such a companion, depending on its location within the PFN field of view. At each baseline orientation, we compute the difference between the observed null and the value expected from the LD photospheric model above. This provides an estimate of the "excess leakage," and of its 3σ upper limit. This excess limit is then converted into a point source flux limit using the PFN sky transmission grid (Figure 1). Such upper flux limit maps are derived for each of the three baseline orientations. At any given location in α Her's immediate environment probed by the instrument (about 300 mas or 33 AU in radius), only the lowest of these three limits is retained. This yields the final map presented in Figure 6, showing the maximum (relative) K-band flux of a companion as a function of its location around α Her. At the very center of the field, within 1 AU of the central star, the contribution of any off-axis source would be nulled out, and so no useful flux constraint can be derived. Similarly, the PFN data do not reflect emission from sources located further than $\simeq$30 AU, i.e., beyond the single-mode fiber field of view. Our data are most sensitive to the central (2–10 AU) region where we can rule out the presence of any companion contributing more than 2% of α Her's overall K-band flux at the time of the observations.

4.1.3. β And

β And is an M0 giant with a temperature of 3800 K and $\log g = 1.5$, and a predicted limb darkening K-band coefficient of 0.383 (Claret et al. 1995). The PFN measured a null value of $7.0 \times 10^{-3} \pm 9 \times 10^{-4}$, yielding (Equation (A4))

[4] Fiber Linked Unit for Optical Recombination/Infrared and Optical Telescope Array.

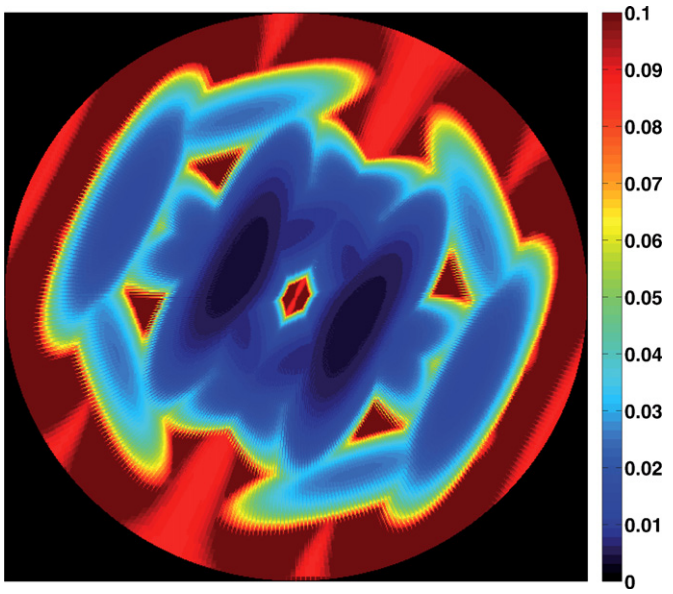

Figure 6. Upper limits (3σ) to the relative K-band flux contributed by a companion around α Her, depending on its location. North is up, east is to the left, field-of-view radius is 300 mas ($\simeq$33 AU). Based on 2009 July 10 PFN data recorded at three different baseline orientations spanning 90 deg in azimuth. As expected, constraints on a putative companion get looser at the edge of the fiber field of view, and at the center of the field, where destructive interference occurs for all baseline orientations.

(A color version of this figure is available in the online journal.)

an LD diameter of 15.29 mas $\pm$ 0.99 mas. In comparison, the LD diameter measured by LBI is 14.35 mas $\pm$ 0.19 mas (Di Benedetto & Rabbia 1987), yielding an expected null depth of $6.2 \times 10^{-3} \pm 2 \times 10^{-4}$. The PFN and LBI measurements consequently agree at the 1σ level.

4.1.4. Capella

α Aurigae (Capella) is a bright nearby (12.9 pc) binary system (G8III/G1III), with the two components close to equally bright in the visible. We measure for the system a null depth value of $5.2 \times 10^{-2} \pm 4 \times 10^{-3}$. The most recent parameters derived from radial velocity measurements (Torres et al. 2009) provide a primary diameter of 8.50 mas and a secondary diameter of 6.27 mas, with respective effective temperatures of 4920 K and 5680 K. Assuming blackbody emission, this yields a K-band secondary to primary flux ratio $r = 0.70$. At the time of the PFN observations (Besselian epoch = 2008.8666), the derived (Hartkopf & Mason 2006) separation is 41.5 mas for an azimuth of 135.5 deg east of north. This is 63.5 deg with respect to the single PFN baseline orientation used. Using these orbital parameters together with the stellar data from Torres et al., Equations (8) and (A5) yield a predicted null depth of 5.1×10^{-2} for this binary system, in very good agreement with our observed value. It is worth noting that if Capella A had been the only star in the fiber's field of view, the observed astrophysical null would have been only 2.3×10^{-3}. This illustrates the PFN's ability to detect companions well within the diffraction limit.

4.2. Individual Results: Mass-losing Stars

4.2.1. β Peg

β Peg is an M2.5II-III pulsating variable giant, with an effective temperature of 3600 K and $\log g = 1.2$, and a predicted limb darkening coefficient of 0.389 (Claret et al. 1995). A significant null depth variation is detected between the two PFN azimuth positions. At 87 deg azimuth angle, the observed null depth is $8.9 \times 10^{-3} \pm 4 \times 10^{-4}$, corresponding to an apparent LD diameter of 17.25 mas $\pm$ 0.39 mas. At 117 deg the astrophysical null depth increases to $1.13 \times 10^{-2} \pm 7 \times 10^{-4}$, and the apparent LD diameter increases to 19.43 mas $\pm$ 0.61 mas. For comparison, the LD diameter derived for this object from previous LBI measurements is 16.75 mas $\pm$ 0.24 mas (Di Benedetto & Rabbia 1987). This corresponds to an astrophysical null of $8.4 \times 10^{-3} \pm 2 \times 10^{-4}$, in good agreement with our first azimuth measurement. However, our second measurement shows significant (4.1σ) extra leakage with respect to LBI predictions, and points to asymmetries at the $\simeq$10% level. This could be either due to extended atmospheric layers or to the presence of a companion contributing at least 3×10^{-3} of the K-band flux. Interestingly, β Peg is already known to host a warm ($\simeq$1500 K) H_2O upper outside layer, with column density of the order of 2×10^{18} molecules cm^{-2} (Tsuji et al. 2001). Rather than photospheric asymmetries, the observed K-band null depth variations could then reflect variations of the upper molecular layer's opacity with respect to azimuth.

4.2.2. α Ori

α Ori is a famous and well-studied semi-regular pulsating bright supergiant (type M2Iab). It was observed under poor seeing conditions in 2008 November with the initial PFN set-up, yielding a larger measurement uncertainty than for most stars in the sample. From three separate data sets, we derive an astrophysical null depth of $8.1 \times 10^{-2} \pm 4 \times 10^{-3}$. In comparison, two separate limb darkening measurements of α Ori's photosphere have been obtained through long baseline near-infrared interferometric observations at IOTA. Measurements carried at K band (Perrin et al. 2004) and H band (Haubois et al. 2009) yielded fairly identical LD diameters (respectively 43.65 $\pm$ 0.10 mas and 44.28 $\pm$ 0.15 mas), while the best-fit linear limb darkening coefficients varied from 0.09 (K-band data) to 0.43 (H-band data). Using Equations (8) and (A2), these two separate measurements translate into fairly similar photospheric null depths at the PFN's baseline: $6.10 \times 10^{-2} \pm 3 \times 10^{-4}$ and $5.92 \times 10^{-2} \pm 4 \times 10^{-4}$.

The value measured by the PFN is significantly higher than either of these measurements, pointing to some extra source of emission above the photosphere. A possibility is specifically the "MOLsphere" model suggested by Perrin et al. for this star, which incorporates an upper geometrically thin molecular layer at 2050 K, located 0.33 stellar radii above the photosphere with a 0.06 K-band opacity. Simulating the spherically symmetric brightness distribution corresponding to this two-component model (see Equations (9) and (10) of Perrin et al. 2004), and computing the resulting visibility, the derived PFN null depth only increases to 6.3×10^{-2}. The properties of such a layer may obviously have changed since the IOTA observations (K band: 1996–1997, H band: 2005), and our single baseline measurement does not allow the various parameters to be individually retrieved. As an illustration, an upper layer with the same characteristics but located at a higher altitude (0.88 R^*) would reproduce the observed 8.1×10^{-2} null depth. Finally, our observed null excess is also consistent with the more recent near-infrared (J, H, and K band) AO assisted measurements of α Ori obtained with the Very Large Telescope/NACO[5] instrument (Kervella et al. 2009), which partially resolved a complex

[5] NACO: NAOS/CONICA (NAOS: Nasmyth Adaptive Optics System; CONICA: Near-Infrared Imager and Spectrograph).

asymmetric circumstellar environment. Further observations at different PFN baseline orientations would then be very informative, particularly around a position angle of 200° where a significant envelop extension ("plume") was detected by Kervella et al.

4.2.3. ρ Per

ρ Per is an M4II semi-regular variable star with an effective temperature of ≃3500 K and $\log g = 0.8$, with an estimated limb darkening *K*-band coefficient of 0.394 (Claret et al. 1995). The PFN measures an astrophysical null value of $7.4 \times 10^{-2} \pm 7 \times 10^{-3}$, which is considerably larger than the value of $8.4 \times 10^{-3} \pm 2 \times 10^{-4}$ expected using its measured LD diameter of 16.75 mas ± 0.24 mas (Di Benedetto & Rabbia 1987). This is the largest excess above photospheric emission observed among the stars in our sample, pointing to a possible recent mass loss event since the measurements reported by Di Benedetto & Rabbia. Further observations are required to constrain the source of extra emission. Extended outer molecular layers are expected around this kind of semi-regular M giant. They are a likely explanation for the PFN measured excess since no bright companion is presently known around ρ Per.

4.2.4. χ Cyg

χ Cyg is a well-studied S-type Mira star, with extended upper atmospheric molecular layers (mostly CO in our bandpass) evidenced by many high spatial resolution observations (Young et al. 2000; Mennesson et al. 2002b; Lacour et al. 2009). The PFN measured astrophysical null is $2.9 \times 10^{-2} \pm 2.5 \times 10^{-3}$. In order to compare this result to previous LBI measurements, we use the observations of Lacour et al., who have used the IOTA interferometer in *H* band to measure precise time-dependent values of the stellar diameter, and evidenced the presence and displacement of a warm molecular layer. According to the IOTA measurements, the stellar diameter, corrected for limb darkening, has a mean value of 24.2 mas and shows a 10.2 mas amplitude pulsation. Using the sinusoidal fit of diameter versus phase derived from these observations, we predict an LD diameter of 23.24 mas at the time of the PFN measurements (variability phase = 0.72). Adopting at *K* band the same limb darkening power law as was measured in *H* band by Lacour et al. ($\alpha \simeq 2.5$), and using Equations (8) and (A2), the expected null leakage from χ Cyg's photosphere would be 1.66×10^{-2} at the PFN baseline. Assuming instead that there is no limb darkening in the *K* band, the null increases to 1.73×10^{-2}. This provides an upper limit to the null expected from the photosphere alone. In comparison, the PFN measures a significantly larger null value. This excess leakage likely reflects extra emission from the circumstellar layers detected by high-resolution spectral measurements (Hinkle et al. 1982) and by LBI. We thus next consider the two-component model derived by Lacour et al. at a pulsation phase of 0.72, consisting of a central 2500 K photosphere (same diameter as above), surrounded by a single 1800 K spherical molecular layer (35 mas in diameter). Using this model, we find that the PFN measured null depth can be reproduced when setting the outer layer *K*-band optical depth to 0.07. This is perfectly aligned with the optical depth values derived at *H* band by Lacour et al. at phases similar to that of our observations: 0.067 at phase 0.69, and 0.074 at phase 0.79.

4.3. Discussion

Figure 7 summarizes our results by comparing the stellar nulls measured by the PFN to the null depths predicted by

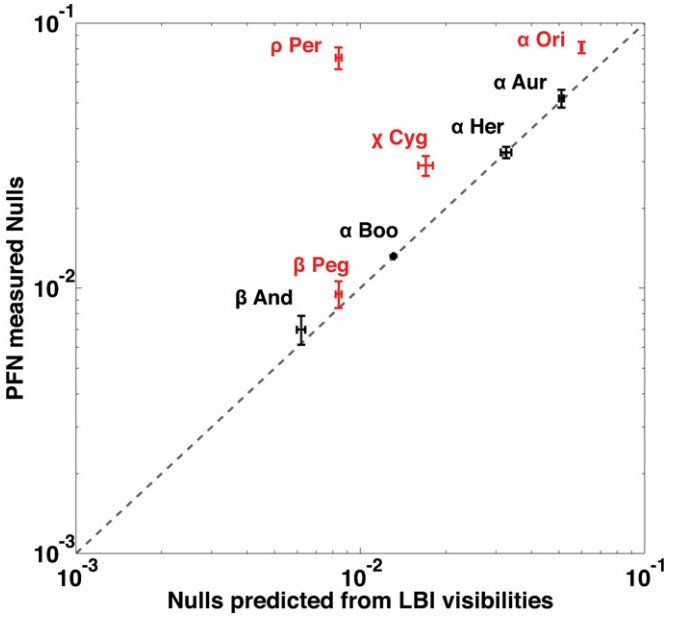

Figure 7. Stellar nulls measured by the Palomar Fiber Nuller compared to values expected from near-IR long baseline interferometry (LBI) and stellar modeling (photosphere only): α Boo (Perrin et al. 1998; Lacour et al. 2008), α Her (Perrin et al. 2004), β Peg (Di Benedetto & Rabbia 1987), β And (Di Benedetto & Rabbia 1987), α Ori (Perrin et al. 2004; Haubois et al. 2009), ρ Per (Di Benedetto & Rabbia 1987), α Aur (Torres et al. 2009; Hartkopf & Mason 2006), and χ Cyg (Lacour et al. 2009). Four targets in the sample (indicated in red) are Miras or semi-regular variable stars known to exhibit extended outer molecular and dust shells above their photosphere. The PFN detects significant departure from naked photosphere models for three of them (α Ori, ρ Per, and χ Cyg), while substantial asymmetry is detected around β Peg. The large discrepancy measured on ρ Per suggests a recent mass loss event. Note that due to the logarithmic scaling, a given error bar appears larger around low null values.

(A color version of this figure is available in the online journal.)

near-infrared LBI measurements of the stellar photospheres. The agreement is excellent for "standard" giants and supergiants (α Boo, α Her, and β And) and for the well-studied binary system α Aur. In all four cases, the discrepancy between the observed and expected null values is smaller than 0.1%, and well within the error bars derived from the PFN and LBI measurements. Using these four stars, the weighted mean difference between the two types of measurements (PFN−LBI) is $+ 2.1 \times 10^{-4}$, with a weighted standard deviation of 3.1×10^{-4}. These overall results indicate that the fiber nulling approach produces accurate null (visibility) measurements, with no detectable bias down to the few 10^{-4} level. This complements our previous precision estimation based on α Boo data alone (Hanot et al. 2011) and confirms the overall conclusion that the fiber nuller data acquisition and reduction strategies allow very accurate null (and visibility) measurements. Furthermore, without any observation of calibrator stars, the typical accuracy is already about an order of magnitude better than that obtained by long baseline interferometers, whose best reported null accuracy is 0.2% in the mid-infrared (Colavita et al. 2009) and about 0.25% in the near-infrared (i.e., 0.5% rms visibility accuracy Kervella et al. 2004).

Furthermore, significant departure from centrally symmetric naked photosphere models is detected for the four variable, mass-losing stars in our sample. Clear excesses are detected around α Ori and χ Cyg, with values consistent with previous LBI observations of extended outer molecular layers around these stars. A small excess and variation versus azimuth is

detected on β Peg. The large excess measured on ρ Per suggests a recent significant mass loss event or some previously undetected companion and is reported here for the first time.

The overall consistency of the PFN short baseline results with those obtained by much larger arrays illustrates the point that accurate null measurements do not only provide better contrast. They also provide better spatial resolution for a given baseline since smaller sources can be reliably resolved and characterized.

5. CONCLUSIONS AND PERSPECTIVES

Very precise stellar null (or visibility) measurements have been demonstrated at Palomar in the near-infrared using a fiber nuller and a new statistical data analysis technique. In an effort to assess the absolute accuracy of the method, we have compared our results to those provided by LBI on eight bright giants and supergiants. For "naked stars," for which no circumstellar excess emission was previously detected, our results are consistent with high-resolution photospheric measurements from LBI at the few 10^{-4} level. For all of the mass-losing stars observed, we detect either slight asymmetries (at the 2–3 $\times$ 10^{-3} level around β Peg) or excess emission above the photosphere (at the $\simeq 10^{-2}$ level around α Ori and χ Cyg, and at much higher level around ρ Per). These results, obtained with a 3.2 m baseline, illustrate the points that (1) accurate null measurements are achievable in the near-infrared in spite of much larger phase fluctuations than in the mid-infrared, and (2) accessing better contrast also provides better spatial resolution for a given baseline.

With the Palomar extreme AO system coming online in 2011 (Bouchez et al. 2011), and with a new state-of-the-art science camera becoming available, simulations indicate that contrasts of the order of 10^{-4} to 10^{-3} should be obtainable with the PFN on $m_K = 6$ stars as close as 30 mas from the axis. We can test this prediction and further assess the accuracy limits of the system by observing well-known high-contrast binary systems, as well as calibrator stars. Moreover, we can use the PFN to carry out a survey of hot dust populations similar to those recently inferred by LBI, but with a higher dynamic range than previously available, typically 10^{-3} or better. The PFN is particularly adapted to the study of bright debris disks around nearby A stars, as recently evidenced by our high-contrast observations of Vega's inner few AU (Mennesson et al. 2011).

This work was performed at the Jet Propulsion Laboratory, California Institute of Technology, under contract with NASA. The data presented are based on observations obtained at the Hale Telescope, Palomar Observatory, as part of a continuing collaboration between Caltech, NASA/JPL, and Cornell University. We thank the Palomar Observatory staff for their assistance in mounting the PFN and conducting the observations at the Hale telescope.

APPENDIX

ASTROPHYSICAL NULL DEPTH EXPRESSIONS

Denoting by $I(\vec{\theta})$ the observed sky brightness distribution, including both the source spatial brightness distribution and the lobe antenna of the fiber, the object complex visibility V is defined as

$$V(\lambda) = \frac{\int I(\vec{\theta}) e^{(j.2\pi \vec{B}.\vec{\theta}/\lambda)} d\vec{\theta}}{\int I(\vec{\theta}) d\vec{\theta}}, \quad \text{(A1)}$$

where B is the interferometric baseline and λ the observing wavelength. In the case of the PFN, B corresponds to the center-to-center distance between the two elliptical 1.5 m $\times$ 3 m sub-apertures of the primary 5 m diameter mirror. Based on the optical model of the telescope and on engineering data, the PFN interferometric baseline is 3.20 m $\pm$ 0.01 m. As for the observing wavelength, PFN measurements are made in a waveband covering 2.05 to 2.35 μm. Based on the detector chromatic efficiency and the K-band filter transmission curve, the effective (center) wavelength of the PFN is determined to be $\lambda = 2.16\,\mu$m. This effective wavelength exhibits very small variations (<3 nm) versus stellar temperature, and is therefore assumed constant for all stars considered here.

When the object is centrally symmetric, one obtains (using Equation (8))

$$N^a(\lambda) = \frac{\int I(\vec{\theta}) \sin^2(\pi \vec{B}.\vec{\theta}/\lambda) d\vec{\theta}}{\int I(\vec{\theta}) d\vec{\theta}}. \quad \text{(A2)}$$

In particular, for a naked star represented by a uniform disk of diameter $\theta^* \ll \lambda/B$, the observed astrophysical null depth is given by

$$N^a(\lambda) = \left(\frac{\pi B \theta^*}{4\lambda}\right)^2. \quad \text{(A3)}$$

For a more realistic model, in which a naked star is represented by a limb darkened disk of diameter $\theta^{\rm LD}$, with a linear limb darkening coefficient $A(\lambda)$, the observed astrophysical null depth is (Absil et al. 2011)

$$N^a(\lambda) = \left(\frac{\pi B \theta^{\rm LD}}{4\lambda}\right)^2 . \left(1 - \frac{7A}{15}\right) . \left(1 - \frac{A}{3}\right)^{-1}. \quad \text{(A4)}$$

Finally, for a binary source, one still has $N^a = (1 - |V|)/(1 + |V|)$, and the complex visibility V (Equation (A1)) given by

$$V = \frac{V_1 + r.V_2.e^{(j.2\pi \vec{B}.\vec{\theta}_{1-2}/\lambda)}}{1 + r}, \quad \text{(A5)}$$

where V_1 and V_2 are the visibilities derived for each of the two stars, r is their flux ratio at the observing wavelength, and $\vec{\theta}_{1-2}$ is their angular separation.

REFERENCES

Absil, O., di Folco, E., Mérand, A., et al. 2006, A&A, 452, 237
Absil, O., den Hartog, R., Gondoin, P., et al. 2011, A&A, 527, 4
Angel, J. R., Burge, J. H., & Woolf, N. J. 1997, Proc. SPIE, 2871, 516
Boccaletti, A., Carbillet, M., Fusco, T., et al. 2008, Proc. SPIE, 7015, 177
Boccaletti, A., Riaud, P., Baudoz, P., et al. 2004, PASP, 116, 1061
Bouchez, A., Dekany, R. G., Angione, J. R., et al. 2008, Proc. SPIE, 7015, 24
Claret, A. 2000, A&A, 363, 1081
Claret, A., Diaz-Cordoves, J., & Gimenez, A. 1995, A&AS, 114, 247
Colavita, M., Serabyn, E., Millan-Gabet, R., et al. 2009, PASP, 121, 1120
Di Benedetto, G. P., & Rabbia, Y. 1987, A&A, 188, 114
Duvert, G., Chelli, A., Malbet, F., & Kern, P. 2010, A&A, 509, 66
Haguenauer, P., & Serabyn, E. 2006, Appl. Opt., 45, 2749
Hanot, C., Mennesson, B., Martin, S., et al. 2011, ApJ, 729, 110
Hartkopf, W. I., & Mason, B. D. 2006, Sixth Catalog of Orbits of Visual Binary Stars (Washington, DC: USNO) (http://ad.usno.navy.mil/wds/orb6.html)
Haubois, X., Perrin, G., Lacour, S., et al. 2009, A&A, 508, 923
Hinkle, K. H., Hall, D. N. B., & Ridgway, S. T. 1982, ApJ, 252, 697
Hinkley, S., Oppenheimer, B. R., Soummer, R., et al. 2007, ApJ, 654, 633
Kalas, P., Graham, J. R., Chiang, E., et al. 2008, Science, 322, 1345
Kervella, P., Coudé du Foresto, V., Segransan, D., & di Folco, E. 2004, Proc. SPIE, 5491, 741
Kervella, P., Verhoelst, T., Ridgway, S. T., et al. 2009, A&A, 504, 115
Lacour, S., Meimon, S., Thiébaut, E., et al. 2008, A&A, 485, 561
Lacour, S., Thiébaut, E., Perrin, G., et al. 2009, ApJ, 707, 632
Liu, M. C., Wahhaj, Z., Biller, B., et al. 2009, in AIP Conf. Proc. 1094, Cool Stars, Stellar Systems and the Sun (Melville, NY: AIP), 461

Marois, C., Macintosh, B., Barman, T., et al. 2008, Science, 322, 1348
Marois, C., Macintosh, B., Soummer, R., Poyneer, L., & Bauman, B. 2008, Proc. SPIE, 7015, 47
Martin, S., Serabyn, E., Liewer, K., et al. 2008, Proc. SPIE, 7013, 57
McAlister, H. A. 1993, AJ, 106, 4
Mennesson, B., Crawford, S. L., Serabyn, E., et al. 2003, in Proceedings of the Conference on Towards Other Earths: DARWIN/TPF and the Search for Extrasolar Terrestrial Planets, ed. M. Fridlund & T. Henning (Noordwijk: ESA), 525
Mennesson, B., Haguenauer, P., Serabyn, E., & Liewer, K. 2006, Proc. SPIE, 6268, 95
Mennesson, B., Ollivier, M., & Ruilier, C. 2002a, J. Opt. Soc. Am. A, 19, 596
Mennesson, B., Perrin, G., Chagnon, G., et al. 2002b, ApJ, 579, 446
Mennesson, B., Serabyn, E., Hanot, C., Martin, S., Liewer, K., & Mawet, D. 2011, ApJ, 736, 14
Perrin, G., Coudé du Foresto, V., Ridgway, S. T., et al. 1998, A&A, 331, 619
Perrin, G., Ridgway, S. T., Coudé du Foresto, V., et al. 2004, A&A, 418, 675
Serabyn, E., Mawet, D., & Burruss, R. 2010, Nature, 464, 1018
Torres, G., Claret, A., & Young, P. A. 2009, ApJ, 700, 1349
Troy, M., Dekany, R. G., Brack, G., et al. 2000, Proc. SPIE, 4007, 31
Tsuji, T. 2001, A&A, 376, L1
Young, J. S., Baldwin, J. E., Boysen, R. C., et al. 2000, MNRAS, 318, 381
Zhao, M., Monnier, J. D., ten Brummelaar, T., Pedretti, E., & Thureau, N. D. 2008, Proc. SPIE, 7013, 45